Asymptotic eigensolutions of fourth and sixth rank octahedral tensor operators

William G. Harter and Chris W. Patterson

Citation: Journal of Mathematical Physics **20**, 1453 (1979); doi: 10.1063/1.524199
View online: http://dx.doi.org/10.1063/1.524199
View Table of Contents: http://scitation.aip.org/content/aip/journal/jmp/20/7?ver=pdfcov
Published by the AIP Publishing

Asymptotic eigensolutions of fourth and sixth rank octahedral tensor operators

William G. Harter[a)]

Joint Institute for Laboratory Astrophysics, University of Colorado and National Bureau of Standards, Boulder, Colorado 80309

Chris W. Patterson

University of California, Los Alamos Scientific Laboratory, Los Alamos, New Mexico 87545
(Received 23 August 1978)

Qualitative and quantitative features of high quantum rotational spectra are discussed by appealing to geometrical and topographical representations of the tensor operators. Approximate formulas are derived for level-cluster energies. The approximate conditions for the occurrence of "anomalous" fourfold clusters are given.

I. INTRODUCTION

Eigensolutions of fourth-rank octahedral tensor operators (T^4) have become very useful for analyzing high-resolution laser spectra of heavy spherical top molecules[1,2] such as CF_4, SiF_4, and SF_6.[3] The operators model the centrifugal distortion effects of the molecules which show up in the fine structure patterns in the rotational or rovibrational spectra. Because of high rotational inertia of these molecules their most easily observed lines belong to high rotational quanta typically $J = 10$–100 and higher in some cases. The high J lines are arranged into surprising patterns of spectral "clusters," and the understanding of the clusters has led to simpler theories and better understanding of these molecules.

It is interesting to note that the first observations of clusters were made in computer studies of crystal field splitting of rare earth atomic levels. Lea, Leask, and Wolf [4] used a computer to investigate the effect of adding varying amounts of the sixth rank (T^6) tensor operator to the fourth rank tensor (T^4). They noticed some unexpected triple point degeneracies in their energy level diagrams even for low angular momentum states. (They treated $J \leqslant 8$ only.) Ten years later Dorney and Watson[5] diagonalized T^4 for $J \leqslant 20$ and noted many nearly degenerate clusters for the higher J, and gave a classical model to explain some properties of them. Finally, Fox, Galbraith, Krohn, and Louck[6] performed computer diagonalization of T^4 for $J = 2$–100 and observed many extraordinary properties of clusters. This led to the quantum theory of spectral clusters, parts of which will be reviewed briefly below.[7–11]

The purpose of this article is to continue the original investigation by Lea *et al.*[4] of the effects of adding varying amounts of sixth rank tensor T^6 to T^4. The results of cluster theory will be used and asymptotic formulas will be derived for the limiting cases of high J. The analysis of effects due to tensors of rank six or higher is important for the light spherical tops such as CH_4 (methane), SiH_4 (silane), or GeH_4 (germane) which have appreciable amounts of T^6 in their model Hamiltonians. While there are far fewer light (hydride) tops we believe they may make up for their small number with interesting spectroscopic effects. We shall try to emphasize the intuitive physical nature of the cluster eigenstates and indicate what effects one might predict.

II. TENSOR OPERATORS AND THEIR EIGENVALUES

Rank-k irreducible tensorial operators $T^k_q (q = k, k-1, \ldots, -k)$ of the rotational group R_3 are sets of $2k+1$ operators which transform as follows[12]

$$R(\alpha\beta\gamma) T^k_q R^{-1}(\alpha\beta\gamma) = \sum_{q'} T^k_{q'} \mathscr{D}^k_{q'q}(\alpha\beta\gamma), \tag{1}$$

where $\mathscr{D}^k_{q'q}$ are irreducible representations of rotation operators in $R_3 = \{\cdots R(\alpha\beta\gamma)\cdots\}$. Certain combinations of certain T^k_q are invariant to the subgroup of octahedral rotations. Besides the trivial case T^0_0 we shall consider the two lowest rank octahedral invariants

$$\hat{T}^4 = (7/12)^{1/2} T^4_0 + (5/24)^{1/2}(T^4_4 + T^4_{-4}) \tag{2}$$

and

$$\hat{T}^6 = (1/8)^{1/2} T^6_0 - (\sqrt{7}/4)(T^6_4 + T^6_{-4}). \tag{3}$$

Here we have chosen axes of quantization to be the fourfold symmetry axes of the octahedral subgroup. Many texts[13] give procedures for deriving invariant operators. Instead of giving derivations we shall show ways to picture the operator so that their octahedral symmetry is obvious.

The operators T^4 and T^6 can be expressed in terms of polynomials of coordinate operators x, y, and z or else angular momentum operators J_x, J_y, and J_z. This is done by replacing each T^k_q with spherical harmonics $Y^k_q(\theta,\phi) = Y^k_q(x/r, y/r, z/r)$ or else angular momentum harmonics $Y^k_q(J_x, J_y, J_z)$. Using spherical harmonics we obtain

$$\hat{T}^4 = (21/\pi)^{1/2}[(35\cos^4\theta - 30\cos^2\theta + 3) + 5\sin^4\theta\cos^4\phi]/32 \tag{4a}$$

$$= (7/3\pi)^{1/2}(15)[x^4 + y^4 + z^4 - (3/5)r^4]/8r^4 \tag{4b}$$

and

[a)]Presently at The School of Physics, Georgia Institute of Technology, Atlanta, Georgia 30332.

 0022-2488/79/071453-07$01.00

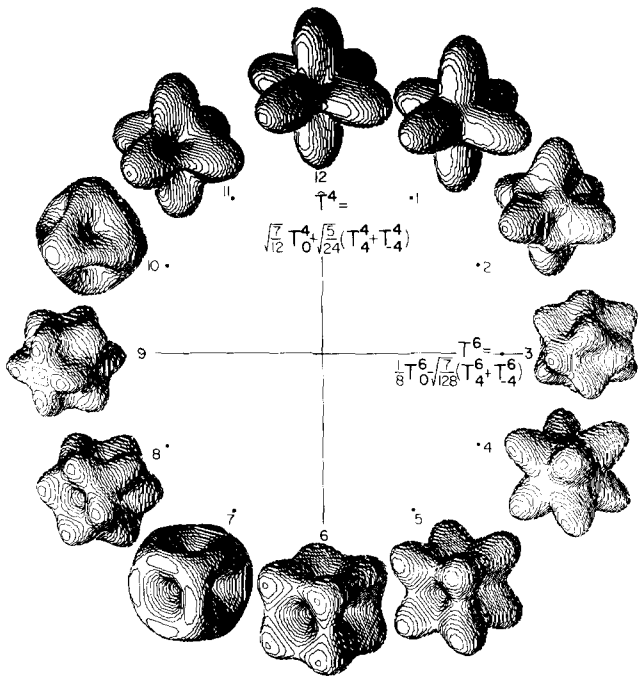

FIG. 1. Geometrical representations of octahedral tensor $T(\mu) = \hat{T}^4 \cos\mu + T^6 \sin\mu$ $[T^6 = (1/\sqrt{8})\,\hat{T}^6]$. Each combination $T(\mu)$ for $\mu = 0,\pi/6,2\pi/6,\ldots,11\pi/6$ is drawn in spherical coordinates $[r = 1 + 1.2T(\mu,\theta,\phi)]$ using (2), (3), (4a), and (5a). Drawings were made on a computer using codes and algorithms written by Chela Kunasz and Thomas Wright.

$$\hat{T}^6 = (104/\pi)^{1/2}[(231\cos^6\theta - 315\cos^4\theta + 105\cos^2\theta - 5) + 21\sin^4\theta(11\cos^4\theta - 1)\cos^4\phi\,]/256 \tag{5a}$$

$$= (13/2\pi)^{1/2}21[x^6 + y^6 + z^6 - 5(x^4y^2 + y^4x^2 + x^4z^2 + y^4z^2 + z^4x^2 + z^4y^2) + 70x^2y^2z^2 - (5/21)r^2]/40r^6. \tag{5b}$$

Figure 1 shows solid spherical plots of the function

$$T(\mu) = \hat{T}^4\cos\mu + T^6\sin\mu, \tag{6a}$$

where angle μ ranges from zero to 2π in steps of $2\pi/12$ and the nonnormalized operator

$$T^6 \equiv (1/8)^{1/2}\,\hat{T}^6 \tag{6b}$$

is used. The plots of Eqs. (4) to (6) were done on computer by Chela Kunasz using solid graphics software developed at the National Center for Atmospheric Research by Thomas Wright. The octahedral symmetry of the figures is evident if one ignores the "wood grain" which merely stands for the limit of the computer storage resolution. (To obtain hidden line drawings the entire function is first stored numerically.) It is useful to think of each figure as a potential surface. One can imagine the hills and valleys correspond to high and low energies in the octahedrally anisotropic Hamiltonian. Note that diametrically opposed numerals on the clock, i.e., 12 and 6, 1 and 7,··· etc., correspond to potentials that differ only by overall sign, that is, hilltops are interchanged with valley bottoms.

If one is interested in moelcular centrifugal distortion operators then it is appropriate to imagine that each of the twelve objects in Fig. 1 are plotted in $\{J_x J_y J_z\}$ space. For example the 12 o'clock object corresponds to molecule whose energy is highest when rotating around the J_x, J_y, or J_z axes which go through the hilltops, and lowest when the J-vector points out of the valley in the (1,1,1) direction. Each surface gives the energy as a function of *J direction* for fixed total angular momentum

$$J_x^2 + J_y^2 + J_z^2 = \text{const.} \tag{7}$$

An octahedral (XY_6) molecule would be distorted the *least* by centrifugal force when rotating around a fourfold x, y, or z axis since then the force is along or perpendicular to the six stronger radial bonds. Rotation around the (1,1,1) or threefold axis affects the weaker bending bonds and causes the greatest distortion. Greater distortion corresponds to more rotational inertia and hence lower energy. This in turn corresponds to a valley on the potential surface. Therefore the surfaces around the 12 o'clock position are apt to describe octahedral XY_6 pure rotational distortion, while their "negatives" around 6 o'clock are more apt to describe cubic (XY_8) or tetrahedral (XY_4) rotational distortion. Note that tetrahedral symmetry alone would allow a third-rank invariant

$$T^3 = J_x J_y J_z, \tag{8}$$

but this is excluded according to time reversal symmetry.

The matrices of tensor operators are made using the Wigner–Echart theorem

$$\langle {}^{J}_{M'} | T^k_q | {}^{J}_{M} \rangle = (-1)^{J-M} \begin{pmatrix} J & k & J \\ -M' & q & M \end{pmatrix} (J \| T^k \| J), \tag{9}$$

where the reduced matrix element $(J\|T^k\|J)$ can be taken outside of the matrix since it does not depend on M or M'. We shall set it equal to unity here, but its value can be computed once the exact form of the tensor operator is established. The other factor in (9) is the Wigner 3-j coefficient. The following values of this coefficient are needed:

$$\begin{pmatrix} J & 4 & J \\ -M & 0 & M \end{pmatrix}$$

$$= (-1)^{J-M}[6(J+2:-1) - 10M^2(6J^2 + 6J - 5) + 70M^4]/[(2J+5:-3)]^{1/2}, \tag{10a}$$

$$\begin{pmatrix} J & 4 & J \\ -(M-4) & -4 & M \end{pmatrix} = (-1)^{J-M}[70(J+M+0:-3)(J-M+4:1)]^{1/2}/[(2J+5:-3)]^{1/2}, \tag{10b}$$

$$\begin{pmatrix} J & 6 & J \\ -M & 0 & M \end{pmatrix}$$

$$= (-1)^{J-M}[-20(J+3:-2) + 84M^2(5J^4 + 10J^3 - 20J^2 - 25J + 14) - 420M^4(3J^2 + 3J - 7) + 924M^6]/[(2J+7:-5)]^{1/2} \tag{10c}$$

$$\begin{pmatrix} J & 6 & J \\ -(M-4) & -4 & M \end{pmatrix}$$

$$= 12(-1)^{J-M}(50 - 44M + 11M^2 - J^2 - J)$$

$$\times [(7/2)\,(J + M + 0{:}\,-3)\,(J - M + 4{:}1)]^{1/2}/$$

$$[(2J + 7{:}\,-5)]^{1/2}. \tag{10d}$$

Here we use the notation

$$(X + a{:}b) = (X + a)(X + a - 1)(\cdots)(X + b + 1)(X + b). \tag{11}$$

The angular momentum representation of the (4,6)-octahedral operator

$$T(\nu) = \hat{T}^4 \cos\nu + \hat{T}^6 \sin\nu \tag{12}$$

in the $|^J_M\rangle$ basis is a $(2J+1)\times(2J+1)$ matrix. Using octahedral symmetry adapted bases[1,2] it is possible to reduce it to a direct sum of smaller block diagonal matrices belonging to each symmetry species A_1, A_2, E, T_1, and T_2. For example for $J = 30$ one can reduce the (61×61) matrix to two (3×3) A_1 and A_2 blocks, a (5×5) E block, a (7×7) T_1 block, and an (8×8) T_2 block. Finally 26 distinct eigenvalues (the E- and T-levels are, doubly and triply degenerate, respectively) are obtained in the $(J = 30)$ case by diagonalizing the sub blocks. These blocks can be produced and diagonalized by computer[14] and the results for $J = 30$ are shown in Fig. 2 as a function of parameter ν $(0 \leqslant \nu \leqslant \pi)$. It is only necessary to carry this expensive computer calculation half way around the ν-clock. The eigenvectors of a matrix are unchanged by an overall (-1) factor and the eigenvalues are merely inverted.

We now see ways to understand the results of the diagonalizations and derive simple approximate formulas for the eigenvalues.

III. APPROXIMATIONS FOR TENSOR OPERATOR SPECTRA

The first thing one notes in Fig. 2 is that many of the 26

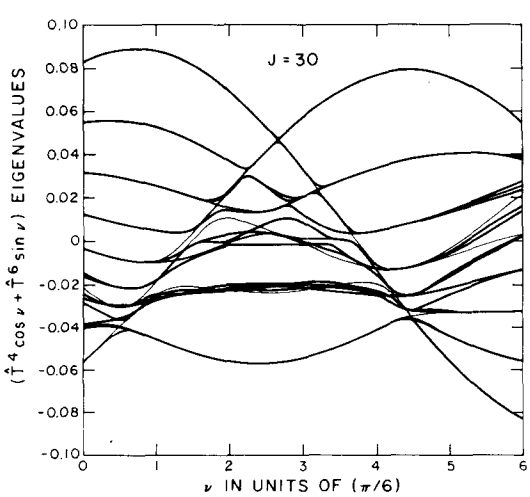

FIG. 2. ($J = 30$) Eigenvalue spectrum of $T(\nu)' = \hat{T}^4 \cos\nu + \hat{T}^6 \sin\nu$.

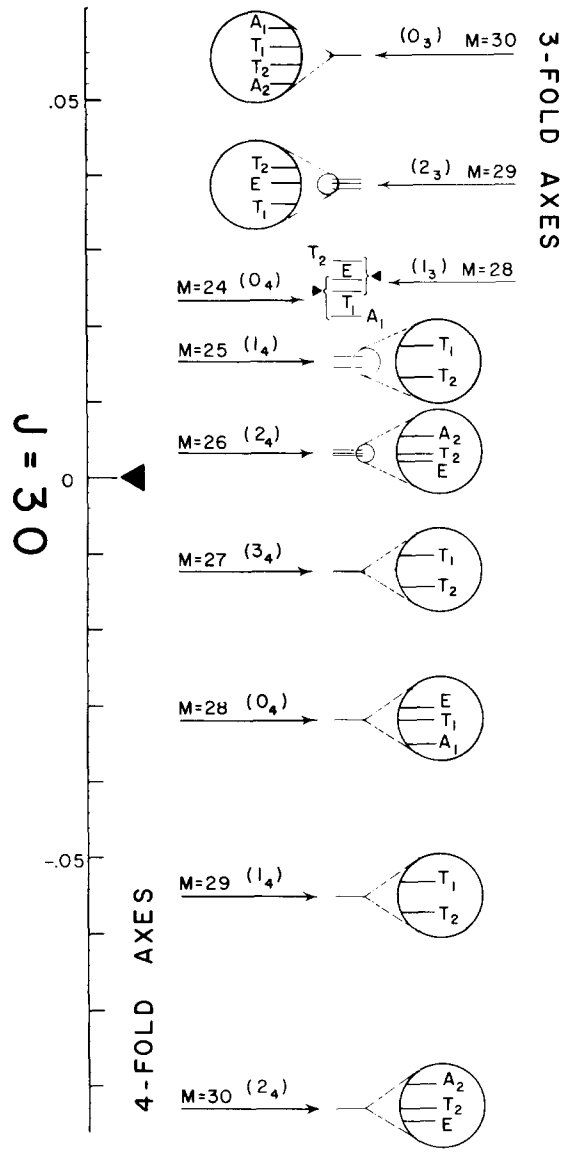

FIG. 3. ($J = 30$, $\nu = \pi$) Spectrum of $T(\nu)$. Magnified view of the level clusters are shown to exhibit the separate octahedral symmetry species.

eigenvalues are "clustering" for most ν values. The spectrum is a good deal simpler than it would have been if all 26 values had been randomly deployed. Figure 3 shows the spectral detail for the extreme right-hand side of Fig. 2, i.e., $\nu = \pi$... [the extreme left-hand side ($\nu = 0$) is just the negative of this]. The lower portion of the spectrum exhibits alternative $(A \oplus T \oplus E)$ and $(T_1 \oplus T_2)$ clusters. Each of these clusters contain six levels: either $1 + 3 + 2 = 6$ or $3 + 3 = 6$. As explained in Refs. 7–9 each set of six levels corresponds to six more-or-less well-defined localized rotation states in each of the six valleys on fourfold axes at 6 o'clock ($\nu = \pi = \mu$) in Fig. 1. The upper portion of the spectra exhibits $(A_1 \oplus T_1 \oplus T_2 \oplus A_2)$ and $(T_1 \oplus E \oplus T_2)$ clusters each containing eight levels. These belong to states sitting in each of eight hills on three-fold axes at 6 o'clock or in each of eight valleys at 12 o'clock ($\nu = 0 = \mu$). Note that the fourfold axial hills or valleys are deeper than the threefold valleys or hills at the 12 o'clock or 6 o'clock positions. Therefore there are more fourfold or six-level clusters than threefold or eight-level

clusters at these positions. However, at just before 4 o'clock ($\mu = 120° = 2\pi/3$, $\nu = \tan^{-1}[(1/8)^{1/2}\tan\mu] = 148.5°$ $= 9.9\pi/12$) or else at 10 o'clock in Fig. 1 the threefold hills or valleys predominate. In the corresponding neighborhood between $\nu = 8\pi$ and $\nu = 10\pi$ in Fig. 2 the threefold clusters dominate the spectrum.

The splitting of a level cluster is determined by how easily tunneling occurs between the valleys or hills associated with the cluster. As explained in Refs. 6–9 and 11 the nearest neighbor tunneling amplitude ($-S$) appears in the ($A_1 \oplus T_1 \oplus E$) cluster eigenvalues

$$E(E) = H + 2S, \tag{13a}$$

$$E(T_1) = H, \tag{13b}$$

$$E(A_1) = H - 4S, \tag{13c}$$

and predicts the observed 2:1 splitting ratio between E-T_1 and T_1-A_1 intervals in the fourfold region of Fig. 3. (Here H is the cluster center-of-gravity which will be discussed shortly.) Similarly, threefold cluster eigenvalues are given by

$$E(A_1) = H + 3S + 3T, \tag{14a}$$

$$E(T_1) = H + S - T, \tag{14b}$$

$$E(T_2) = H - S - T, \tag{14c}$$

$$E(A_2) = H - 3S + 3T, \tag{14d}$$

for the ($A_1 \oplus T_1 \oplus T_2 \oplus A_2$) cluster and for the ($T_1 \oplus E \oplus T_2$) cluster by

$$E(T_2) = H + 2S - T, \tag{15a}$$

$$E(E) = H + 3T, \tag{15b}$$

$$E(T_1) = H - 2S - T, \tag{15c}$$

where S is nearest neighbor tunneling amplitude and T is the *next* nearest neighbor tunneling amplitude. For most threefold clusters the T amplitude is negligible, however there are certain cases when S goes through zero with T nonzero as will be discussed at the end of this section.

The fourfold clusters dominate the spectrum around 7 o'clock in Fig. 1 and, of course, also at the antipodal position of 1 o'clock (1 o'clock corresponds to $\mu = 30°$ or $\nu = 11.53° = 0.77\pi/12$). Note that the "pass" between fourfold valleys becomes higher as one goes from 5 o'clock to 6 o'clock. Finally, just before 7 o'clock the pases get cut off and 6 perfect "craters" are formed around the fourfold valleys. This is close to the ν-value for which the spectrum in Fig. 2 is all fourfold clusters. By 8 or 9 o'clock the "passes" have grown up to form twelve mountains. On the opposite side at 2 or 3 o'clock twelve valleys are visible in Fig. 1. These twelve extrema are the source of the twelve-level two-fold clusters ($A_1 \oplus E_1 \oplus T_1 \oplus 2T_2$) and ($A_2 \oplus E \oplus T_2 \oplus 2T_1$) discussed in Ref. 8. (They also can arise in a ν_3-type coriolis spectrum.[15] The twofold axes are located at saddle points or "passes" on the T^4 surface (12 and 6 o'clock) and these points correspond to crossover regions in the spectrum of Fig. 3 between threefold clusters on the high side and four-fold clusters on the low side. Saddle points do not give rise to clusters since it is possible to travel globally between them without having to rise or fall in energy. Clusters correspond to localized states, only.

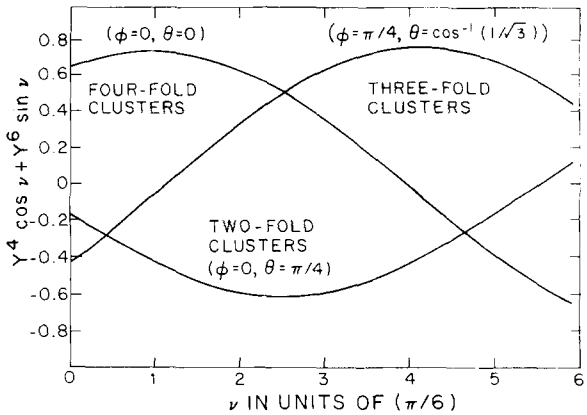

FIG. 4. Local $T(\nu)$ potential values at two-, three-, and fourfold axes. Values of potential $T(\nu) = \hat{T}^4 \cos\nu + \hat{T}^6 \sin\nu$ are plotted versus ν using (4a) and (5a) for select (θ,ϕ) values corresponding to the three kinds of octahedral symmetry axes.

It is instructive to plot the harmonic form of the tensor $T(\nu)$ (12) using (4a) and (5a) for fourfold ($\phi = 0$, $\theta = 0$), threefold [$\phi = \pi/4$, $\theta = \cos^{-1}(1/3)^{1/2}$)], and twofold ($\phi = 0$, $\theta = \pi/4$) axes as in Fig. 4. The qualitative form of the spectrum in Fig. 2 is imitated to some extent. The two-, three-, and fourfold curves mark the regions in which the respective clusters exist. The curves take turns serving as cluster boundaries, i.e., hill tops or valley bottoms, and crossover boundaries, i.e., "passes" at saddle points.

A more accurate approximation of the spectrum is obtained using the matrix elements in (10). If the operators are represented in the appropriate basis then excellent cluster energy approximations are given just by the diagonal components. Even more accurate results are obtained by perturbation. The operators in (2) and (3) are set up in the fourfold basis already. The following zeroth approximation follows:

$$\langle T(\nu)\rangle^0_{4\text{-fold}}$$

$$= (7/12)^{1/2}\begin{pmatrix} J & 4 & J \\ -M & 0 & M \end{pmatrix}(-1)^{J-M}\cos\nu$$

$$+ (1/8)^{1/2}\begin{pmatrix} J & 6 & J \\ -M & 0 & M \end{pmatrix}(-1)^{J-M}\sin\nu, \tag{16}$$

where $M = K_4$ is the fourfold axial momentum associated each cluster. (Recall Fig. 3.) One can do the same for the threefold cluster by first representing (2) and (3) in a threefold axial basis as follows

$$\hat{T}^4 = -2[(7/12)^{1/2}T^4_0 + 2(5/24)^{1/2}(T^4_{-3} - T^4_3)]/3, \tag{17}$$

$$\hat{T}^6 = 2[(8)^{1/2}T^6_0 + (70/24)^{1/2}(T^6_3 - T^6_{-3})$$

$$+ (77/24)^{1/2}(T^6_6 + T^6_{-6})]/9. \tag{18}$$

Then the zeroth threefold cluster approximation is

$$\langle T(\nu)\rangle^0_{3\text{-fold}}$$

$$= -(2/3)(7/12)^{1/2}\begin{pmatrix} J & 4 & J \\ -M & 0 & M \end{pmatrix}(-1)^{J-M}\cos\nu,$$

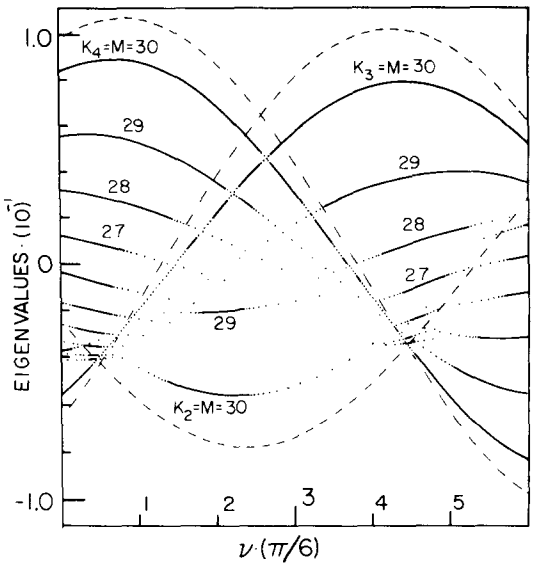

FIG. 5. Approximate ($J = 30$) spectrum of $T(\nu)$. Approximations (16), (19), and (20) are plotted versus ν. Solid lines indicate where there is agreement with the exact results in Fig. 2. Dots indicate where clusters split and approximations break down. Dashed curves corresponds to classical potentials obtained by using (21a) with $P_k = 1$.

$$+ (2/9)(8)^{1/2}\begin{pmatrix} J & 6 & J \\ -M & 0 & M \end{pmatrix}(-1)^{J-M}\sin\nu, \qquad (19)$$

where $M = K_3$ is the threefold cluster momentum. Finally, the zeroth approximation for the twofold clusters is

$$\langle T(\nu)\rangle^0_{2\text{-fold}}$$
$$= -(1/4)(7/12)^{1/2}\begin{pmatrix} J & 4 & J \\ -M & 0 & M \end{pmatrix}(-1)^{J-M}\cos\nu,$$
$$-(13/8))(1/8)^{1/2}\begin{pmatrix} J & 6 & J \\ -M & 0 & M \end{pmatrix}(-1)^{J-M}\sin\nu, \qquad (20)$$

where $M = K_2$ is the twofold cluster momentum. The functions of ν given by (16), (19), and (20) are plotted together in Fig. 5. The solid curves indicate where the agreement is within 2% of the exact results in Fig. 2. This occurs practically everywhere that a cluster exists. In other words, the error is the same order of magnitude as the cluster splitting.

It is interesting to use Edmond's[16] approximate expression

$$\begin{pmatrix} J & k & J \\ -M & 0 & M \end{pmatrix}(-1)^{J-M} = P_k(\cos\theta)/(2J+1)^{1/2}, \qquad (21a)$$

where P_k is a Legendre polynomial and

$$\cos\theta = M/[J(J+1)]^{1/2} \sim M/(J+1/2). \qquad (21b)$$

Its accuracy is about 0.6% at $M = J = 30$ and about 0.05% at $M = J = 100$. It is very useful for helping to understand the classical limit. Let us imagine that the angular momentum in state $|^J_M\rangle$ is represented by a cone of altitude $\langle J_z\rangle = M$ and slant height $\langle J\cdot J\rangle^{1/2} = [J(J+1)]^{1/2} \sim J + 1/2$ about the axis of quantization. According to (21b) the apex half-angle is θ, and according to (21a) the eigenvalue of tensor T^k is proportional to the value of the k th harmonic at angle θ, i.e.,

$$\langle T^k\rangle \propto P_k(\cos\theta)/(2J+1)^{1/2}$$
$$= Y^{k*}_0(\theta)[4\pi/(2k+1)(2J+1)]^{1/2}. \qquad (22)$$

The harmonic valley bottom occurs at $\theta = 0$ where $P_k(1) = 1$. Therefore, if we replace the $3-j$ coefficient and phase in (16), (19), and (20) by $(2J+1)^{-1/2}$ we obtain a better representation than Fig. 4 for the fourfold, threefold, and twofold valley bottoms, hilltops or passes, whichever they might be. These are plotted as dashed lines in Fig. 5. Note that their form is similar apart from the overall magnitude to the topographical features represented by Fig. 4. Any difference is due to the factor $[4\pi/(2k+1)]^{1/2}$ in Eq. (22), which is close to unity for $k = 4$ and 6. Note that even "top clusters" for which $J = M$ have some "zero-point" energy with respect to their valley bottoms or hilltops. This becomes less and less significant as $J \to \infty$.

While studying the asymptotic functional forms of angular coefficients, Ponzano and Regge[17] have deduced "potentials" for Schrödinger-like equations for certain Racah coefficients. Schulten and Gordon[18] have developed a theory of these "potentials" and applied it to approximate derivations of coupling coefficients. The cluster properties seem to point out the physical "reality" of these potentials.

Improved accuracy of the cluster approximation is obtained by using off-diagonal matrix elements in perturbation formulas. This has been done successfully for several cases of fourth-rank tensor operators.[10,15,19] It is interesting to observe that the contribution from the sixth-rank tensor can cause key off-diagonal components to vanish. For example, the key component relating $K_4 = M$ and $K_4 = M - 4$ fourfold cluster states will vanish when

$$(5/24)^{1/2}\begin{pmatrix} J & 4 & J \\ -(M-4) & 4 & M \end{pmatrix}\cos\nu(0)$$

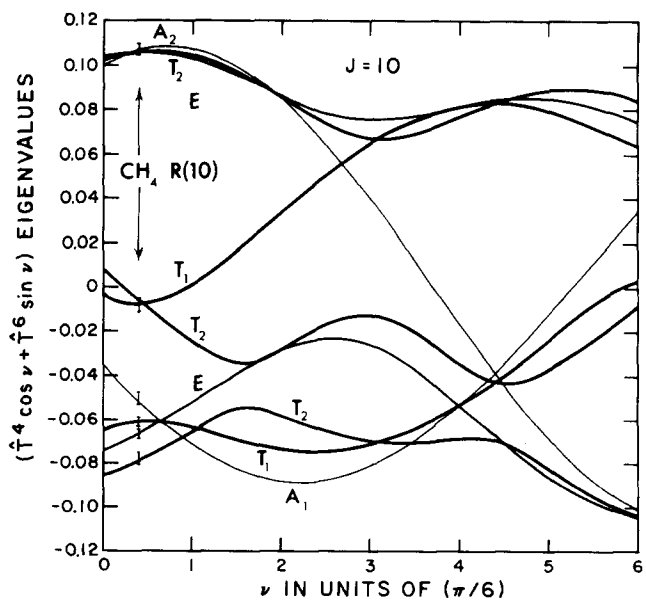

FIG. 6. ($J = 10$) Eigenvalue spectrum of $T(\nu)$.

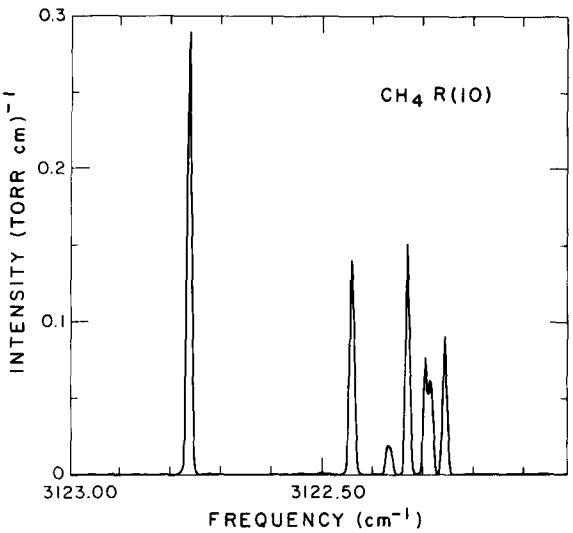

FIG. 7. R (10) Laser spectra of CH_4 (courtesy of Allen S. Pine, MIT Lincoln Laboratory). Symmetry species can be identified by fitting the spectrum with Fig. 6 ($\nu \cong 0.5/6\pi$). This is further verified by the heights of the lines which approximately correspond to the well-known statistical weights: 5 for A_1, 3 for T_1 or T_2, and 2 for E.

$$-(7/16)^{1/2}\begin{pmatrix} J & 6 & J \\ -(M-4) & -4 & M \end{pmatrix}\sin\nu(0) = 0. \tag{23}$$

Solving this using (10) we have

$$\tan\nu_M^J(0) = (5/3)[(2J+7)(2J+6)(2J-4)(2J-5)/42]^{1/2}/$$
$$[50 + 11M(M-4) - J(J+1)]. \tag{24}$$

For example for $J = 10$ one finds the predictions

$$\nu_{10}^{10}(0) = 9.98°, \quad \nu_9^{10}(0) = 13.06°, \quad \nu_8^{10}(0) = 17.74°,$$

which agree rather well with the cluster formations on the left-hand side of Fig. 6. Indeed, it is remarkable that the all fourfold cluster tunneling amplitudes vanish at certain points for each $(A \oplus T \oplus E)$ cluster to give the triple point cluster degeneracies first noticed by Lea *et al.*[4] [Note that the tunneling amplitude corresponding to "reversal"

$$\left(\left|\begin{matrix} J \\ M \end{matrix}\right\rangle \rightarrow \left|\begin{matrix} J \\ -M \end{matrix}\right\rangle\right)$$

is not included in (13)–(15).] The "triple points" for $J = 30$ clusters in Fig. 2 are not resolved on the scale of the graph. However, (24) predicts correctly the values $\nu_{20}^{30}(0) = 16.8°$, $\nu_{21}^{30}(0) = 15.1°$, $\nu_{22}^{30}(0) = 13.7°$, $\nu_{23}^{30}(0) = 12.4°, \ldots, \nu_{30}^{30}(0) = 7.6°$ for which the low-M clusters exist near the fourfold "crater" region around 1 or 7 o'clock (see also Fig. 5).

For threefold clusters there appear points at which the nearest-neighbor tunneling amplitude (S) vanishes while the *next*-nearest-neighbor tunneling amplitude (T) is small but nonzero. The residual (T) exists because of the extra $T^6_{\pm 6}$ terms in (18). This causes the $(T_1 \oplus E \oplus T_2)$ cluster to have a crossing of T_1 and T_2 just below E in the upper right-hand corner of Fig. 6. This was predicted by (15) for $S = 0$ and T small. Similarly, (14) predicts a coincident crossing of A_1 with A_2 and T_1 with T_2 in the $(A_1 \oplus T_1 \oplus T_2 \oplus A_2)$ cluster when $S = 0$. This is seen at ($\nu = 4.4\pi/6$, $E = -0.04$) in Fig. 6. Note just below that crossing there are two levels E and T_2 getting together. This corresponds to part of a cluster falling together in the threefold dominated 4 o'clock (or 10 o'clock) region. The same thing happens to incomplete or "leftover" fourfold clusters in the 1 o'clock (or 7 o'clock) region.

One concludes that sixth rank centrifugal tensors (T^6) can make fourfold clusters anomalously "tight" or degenerate even for lower J, and reorder the structure of threefold clusters. This is important for high resolution spectroscopy since it makes anomalous or case (2) hyperfine structure possible in more accessible regions of the spectrum.[20] The mixing of hyperfine states and symmetry species that inevitably occurs at high J may also happen in select portions of the low J spectrum.

As an example, consider the $J = 10$ spectrum of CH_4 by Pine[21] which is shown in Fig. 7. This fits rather well with the level diagram at about $\nu = 0.9/12\pi$ in Fig. 6. Note that the first ($K_4 = 10$) cluster is very nearly degenerate at this point. The first two fourfold cluster splittings are not resolved in Pine's spectra. Note that the heights of the spectral lines correspond approximately to the well-known nuclear spin statistical weights: 5 for A_1 or A_2, 3 for T_1 or T_2, and 2 for E. The weights "pile up" for clusters so $A_2 + T_2 + E$ is about ten units high in Fig. 7.

More detailed treatments of the molecular Hamiltonian including Coriolis and off-diagonal tensor are needed to fit CH_4 spectra properly, [the P(10) pattern does not fit Fig. 6 well for any value of ν.] One may need also a small amount of eighth rank tensor. However, it appears to be possible to simplify any tetrahedral Hamiltonian calculation by casting it into an appropriate cluster basis for high angular momentum,[11,15,19] and high momentum lines provide the most accurate determination of molecular Hamiltonian constants. Furthermore, the ease with which one can understand and discuss the tensor spectra should be evident. This alone should motivate further development and applications.

ACKNOWLEDGMENTS

We gratefully acknowledge the skilled assistance of Chela Kunasz which was needed to produce the first figure of this article. We also thank the JILA Chairman Dr. David Hummer for making special funds available for this work.

[1] J.D. Louck, thesis, Ohio State University, 1958 (unpublished).
[2] J.M. Bailly, Can. J. Phys. **15**, 237 (1961).
[3] R. McDowell, in *Laser Spectroscopy III*, edited by J.L. Hall and J.L. Carlsten (Springer-Verlag, New York, 1977), p. 102.
[4] K.R. Lea, M.J.M. Leask, and W.P. Wolf, J. Phys. Chem. Solids **23**, 1381 (1962).
[5] A.J. Dorney and J.K.G. Watson, J. Mol. Spec. **42**, 1 (1972).
[6] K. Fox, H.W. Galbraith, B.J. Krohn, and J.D. Louck, Phys. Rev. A **15**, 1363 (1977).
[7] W.G. Harter and C.W. Patterson, Phys. Rev. Lett. **38**, 224 (1977).
[8] W.G. Harter and C.W. Patterson, J. Chem. Phys. **66**, 4872 (1977).
[9] W.G. Harter and C.W. Patterson, Int. J. Quant. Chem. Symp. **11**, 479 (1977).
[10] C.W. Patterson and W.G. Harter, J. Chem. Phys. **11**, 4886 (1977).

[11]W.G. Harter, C.W. Patterson, and F.J. daPaixao, Rev. Mod. Phys. **50**, 37 (1978).
[12]U. Fano and G. Racah, *Irreducible Tensorial Sets* (Academic, New York, 1959).
[13]M. Hammermesh, *Group Theory and Its Applications to Physical Problems* (Addison Wesley, Reading, Massachusetts, 1960).
[14]B.J. Krohn, Los Alamos Report LA-6554-MS, Los Alamos, New Mexico (1976).
[15]W.G. Harter, C.W. Patterson, and H.W. Galbraith, J. Chem. Phys. **69**, 4888–907 (1978).
[16]A.R. Edmonds, *Angular Momentum in Quantum Mechanics* (Princeton U.P., Princeton, New Jersey, 1957), p. 122.
[17]G. Ponzano and T. Regge, in *Spectroscopic and Group Theoretical Methods in Physics*: *Racah Memorial Volume* (North-Holland, Amsterdam, 1968), p. 1.
[18]K. Schulten and R.G. Gordon, J. Math. Phys. **16**, 196 (1975).
[19]H.W. Galbraith, C.W. Patterson, B.J. Krohn, and W.G. Harter, J. Mol. Spectrosc. **73**, 475–93 (1978).
[20]W.G. Harter and C.W. Patterson, in *Advances in Laser Chemistry*, edited by A.H. Zewail (Springer-Verlag, New York, 1978); "Theory of hyperfine and superfine levels in symmetric polyatomic molecules," Phys. Rev. A (submitted).
[21]A.S. Pine, J. Opt. Soc. Am. **66**, 97 (1976).